Pristine graphene as a racemization catalyst for axially chiral BINOL

Asja A. Kroeger,[1] Joel F. Hooper[2,*] and Amir Karton[1,*]

[1]School of Molecular Sciences, The University of Western Australia, Perth, WA 6009, Australia.

[2]School of Chemistry, Monash University, Clayton 3800, Victoria, Australia.

ABSTRACT: Despite versatile applications of functionalized graphene in catalysis, applications of pure, unfunctionalized graphene in catalysis are in their infancy. This work uses both computational and experimental approaches to show that single-layer graphene can efficiently catalyze the racemization of axially chiral BINOL in solution. Using double-hybrid density functional theory (DHDFT) we calculate the uncatalyzed and catalyzed Gibbs free reaction barrier heights in a number of representative solvents of varying polarity: benzene, diphenyl ether, dimethylformamide (DMF), and water. These calculations show that (i) graphene can achieve significant catalytic efficiencies ($\Delta\Delta G^{\ddagger}_{cat}$) varying between 47.2 (in diphenyl ether) and 60.7 (in DMF) kJ mol^{-1}, and (ii) that the catalytic activity is enhanced in polar solvents. An energy decomposition analysis reveals that this catalytic activity is driven by electrostatic and dispersion interactions. Based on these computational results, we explore the graphene-catalyzed racemization of axially chiral BINOL experimentally and show that single-layer graphene can efficiently catalyze this process. Whilst the uncatalyzed racemization requires high temperatures of over 200 °C, a pristine single-layer graphene catalyst makes it accessible at 60 °C.

1. Introduction

Shape complementarity between catalyst and transition structure is one of the cornerstones of chemical catalysis.[1] Equally, non-covalent π-interactions play an increasingly important role in organic, organometallic, and supramolecular catalysis.[2,3,4,5] Pristine graphene has a 2D planar morphology and interacts with surrounding substrates via strong non-covalent π-interactions.[6] These two distinctive properties make pristine graphene an ideal catalyst for chemical processes which proceed via planar transition structures.

Through a series of theoretical studies we recently proposed that unmodified pristine graphene may directly catalyze chemical processes by disproportionately stabilizing shape complementary transition structures over non-planar reactants through non-covalent π-interactions.[7,8] Initial explorations demonstrated computationally that graphene and fragments of graphene may catalyze the bowl-to-bowl inversions of the fullerene fragments corannulene and sumanene,[7,9] as well as the 'flip-flop' inversion of benzo[c]phenanthrene, and the rotation about the C–C bond in substituted biphenyls according to this principle.[7] In a more recent investigation, we showed through extensive density functional theory (DFT) calculations that a $C_{96}H_{24}$ graphene nanoflake may catalyze the racemizations of 1,1′-binaphthyl and 1,1′-binaphthyl-2,2′-diol (BINOL).[8]

BINOL and its derivatives form an important class of chiral ligands and the starting material in the synthesis of a growing family of phosphoric acid organocatalysts.[10,11,12] As such, their enantioselective production remains significant. Hereby, dynamic kinetic resolution forms an attractive alternative synthesis strategy to conventional cross-coupling methods.[13,14,15] However, the high optical stability of many binaphthyl derivatives may hamper such approaches.[16] Recently, Akai and co-workers reported the development of a ruthenium-based racemization catalyst that could be employed effectively in the dynamic kinetic resolution of

BINOL.[14] In this context, it is of interest to explore alternative metal-free recemization catalysts for this process.

The computational results discussed above provide initial indication that pristine graphene may serve as an efficient racemization catalyst.[7,8] What is currently missing from the literature is a study that explores practical aspects of the graphene-catalyzed inversion of BINOL. The present study combines both computational and experimental approaches to investigate this graphene catalysis. We begin by using double-hybrid DFT (DHDFT) methods to explore the uncatalyzed and graphene-catalyzed potential energy surfaces (PESs) of this process in a number of solvents of varying polarity (namely, benzene, diphenyl ether, dimethylformamide, and water). We then perform an energy decomposition analysis (EDA) to identify the nature of the non-covalent interactions responsible for this catalytic activity. Finally, we verify our computational predictions experimentally and show that single-layer graphene can indeed catalyze the inversion of BINOL with near complete racemization after 24 hours at 60 °C, whereas the uncatalyzed reaction requires elevated temperatures of over 200 °C.[17]

2. Computational and Experimental Procedures

Computational details. The geometries and harmonic vibrational frequencies of all structures were obtained from DFT calculations at the PBE-D3BJ/6-31G(d) level of theory.[18,19] Empirical D3 dispersion corrections[20] are included using the Becke–Johnson[21] damping potential (denoted by the suffix D3BJ). Bulk solvent effects in the geometry and frequency calculations were included using the conductor-like polarizable continuum model (CPCM).[22] We consider a number of representative solvents of varying polarity: benzene, diphenyl ether, dimethylformamide (DMF), and water. This level of theory is denoted by CPCM(solvent)-PBE-D3BJ/6-31G(d). The equilibrium structures were verified to have all real harmonic

frequencies and the transition structures (TSs) to have only one imaginary frequency which corresponds to the expected motion along the reaction coordinate. The connectivities of the transition and equilibrium structures were confirmed via intrinsic reaction coordinate (IRC) calculations[23] in the gas-phase at the PBE-D3BJ/6-31G(d) level of theory and these extensive calculations were not repeated in solution due to their high computational cost.[8] We note, however, that the equilibrium and transition structures optimized in solution are similar to those optimized in the gas-phase. All geometry optimizations and frequency calculations were carried out using the Gaussian 16 rev. A.03 program suite.[24]

Double-hybrid DFT calculations were performed using the optimized CPCM(solvent)-PBE-D3BJ/6-31G(d) geometries in order to obtain accurate electronic energies for the equilibrium and transition structures located along the uncatalyzed and catalyzed reaction pathways. Due to the central importance of non-covalent dispersion interactions in the graphene-catalyzed inversion of BINOL, we used the recently developed revDSD-PBEP86-D3BJ DHDFT method, which was developed with non-covalent interaction energies for large systems in mind.[25,26] These calculations were carried out in conjunction with the Def2-TZVPP basis set.[27] All the DHDFT calculations were performed using the ORCA 4.2.0 program suite.[28] Zero-point vibrational energies, enthalpic temperature (H_{298}–H_0), entropic, and bulk solvation corrections were calculated at the CPCM(solvent)-PBE-D3BJ/6-31G(d) level of theory and added to the revDSD-PBEP86-D3BJ electronic energies to obtain the final solution-phase Gibbs free energies at 298 K. This final level of theory is denoted by CPCM(solvent)-revDSD-PBEP86-D3BJ.

To gain further insights into the nature of the non-covalent interactions between the graphene nanoflake and BINOL a second-generation energy decomposition analysis (EDA)[29] based on absolutely localized molecular orbitals (ALMOs) was performed in conjunction with the Def2-SVP basis set.[27] The EDA calculations were carried out with the ωB97M-V exchange

correlation functional[30] in conjunction with the "dispersion-free" Hartree–Fock method as recommended in Ref. 29. These calculations were carried out with the Q-Chem 5.2 program suite.[31,32] All three-dimensional structural representations were generated using the CYLview software.[33]

Experimental details. All solvents, (R)-BINOL and graphene nanoplatelets were purchased from Sigma-Aldrich and used without purification. Single-layer graphene was purchased from ACS Materials. Few-layer graphene was purchased from PlasmaChem GmbH.

(R)-BINOL (30 mg, 0.1 mmol) and single layer graphene (6 mg, 20 wt%) were suspended in a 2:1 mixture of water/DMF (5 mL) and the mixture was stirred at 60 °C for 24 hours. A 100 μL sample of the reaction mixture was diluted with water (1 mL) and extracted with EtOAc (1 mL), and the organic extract was filtered. The organic extract was analyzed by chiral HPLC on a Chirapac OD-H column (6×250 mm), and eluted with 50:50 iPrOH/hexane at 1mL/min, giving an enantiometric ratio of 55:45. (t_1 = 7.54 min, t_2 = 9.46 min.)

3. Results and Discussion

Solvent effects on graphene-catalyzed racemization of BINOL. We begin by examining the uncatalyzed and graphene-catalyzed chirality inversions of BINOL in solution. A number of DFT studies have considered the inversion of binaphthyl derivatives (including BINOL) in the gas-phase[8,34,35,36] and established that racemization consistently proceeds through a kinetically preferred anti-type transition structure with C_i symmetry. Therefore, we focus here on the anti-type reaction pathway. We consider this racemization in representative solvents of varying polarity: benzene (ε = 2.3), diphenyl ether (ε = 3.7), DMF (ε = 37.2), and water (ε = 78.4). Figure 1 gives the molecular geometries obtained along the PES of the catalyzed racemization in DMF and Table 1 summarizes the uncatalyzed and graphene-catalyzed barrier heights for

the racemization of BINOL calculated at the CPCM-revDSD-PBEP86-D3BJ level of theory in these simulated solvents. The calculated reaction barrier height in diphenyl ether for the uncatalyzed reaction (172.1 kJ mol^{-1}) is in good agreement with the recently measured experimental value of 165.4 ± 0.3 kJ mol^{-1}.[17] The relatively small difference of 6.7 kJ mol^{-1} between theory and experiment (i.e., 4.0% of the experimental barrier height) increases our confidence in the chosen level of theory. The gap between theory and experiment may be partially attributed to the inclusion of solvent effects in the calculations via an implicit solvation model.
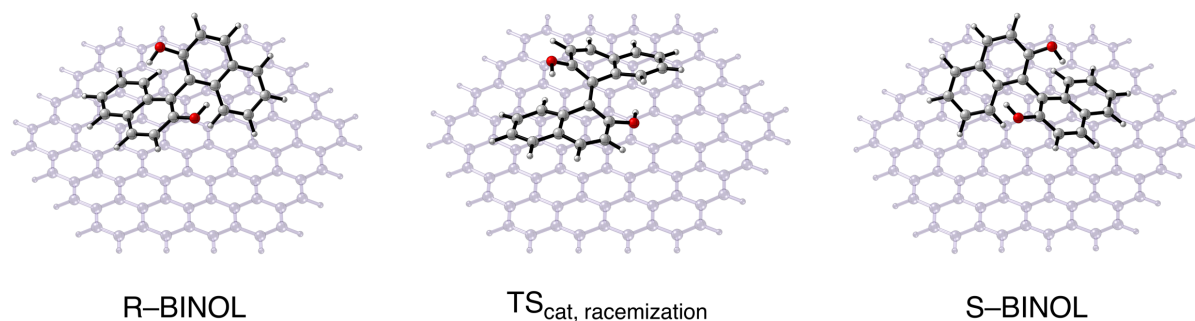

R–BINOL   TS$_{cat, racemization}$ S–BINOL

Figure 1. Reactant complex and transition structure geometries (optimized at the CPCM(DMF)-PBE-D3BJ/6-31G(d) level of theory) located along the graphene-catalyzed PES in DMF.

Table 1. Reaction barrier heights for the uncatalyzed ($\Delta G^{\ddagger}_{uncat}$) and catalyzed ($\Delta G^{\ddagger}_{cat}$) racemizations, and catalytic enhancements ($\Delta\Delta G^{\ddagger}_{cat}$) (CPCM-revDSD-PBEP86-D3BJ, kJ mol^{-1}).

Solvent	ε^{a}	$\Delta G^{\ddagger}_{uncat}$	$\Delta G^{\ddagger}_{cat}$	$\Delta\Delta G^{\ddagger}_{cat}{}^{b}$
Benzene	2.3	171.4	123.6	47.8
Diphenyl ether	3.7	172.1	124.8	47.2
DMF	37.2	173.4	112.7	60.7
Water	78.4	173.5	115.5	58.0

[a]Dielectric constant. [b]$\Delta\Delta G^{\ddagger}_{catalysis} = \Delta G^{\ddagger}_{uncat} - \Delta G^{\ddagger}_{cat}$.

Inspection of the results in Table 1 reveals that the polarity of the solvent has little effect on the uncatalyzed reaction barrier height, with $\Delta G^{\ddagger}_{uncat}$ ranging from 171.4 (benzene, $\varepsilon = 2.3$) to 173.5 (water, $\varepsilon = 78.4$) kJ mol^{-1}. Nevertheless, we note that the barrier heights slightly increase with the dielectric constant of the medium. Solvent polarity has a more pronounced effect on the catalyzed reaction barrier heights. Whereas the reaction barrier heights in the non-polar solvents (benzene and diphenyl ether) are 123.6 and 124.8 kJ mol^{-1}, these barriers are reduced to 112.7 and 115.5 kJ mol^{-1} in the polar solvents (DMF and water).

One quantity that may assist us in analyzing these solvent effects is atomic polar tensor (APT) charges.[37] We note that APT charges, which are based on dipole moment derivatives, have been shown to give a reliable picture of the molecular charge distribution.[38,39] Table S1 of the Supporting Information lists the APT charges on the hydroxyl oxygens and the carbon atoms connected to them in the reactant complex (RC) and catalyzed TS in the four solvents. Examination of these charges reveals that the partial positive charges on the carbon atoms and the partial negative charges on the oxygen atoms are reduced when moving from the RC to the TS. In other words, the polarity of the C–O bond is reduced when moving from the RC to the TS.

The reductions in partial APT charges between the TS and RC are given in Table 2 (denoted by $\Delta APT_{TS-Reac}$ = [APT charge in TS] – [APT charge in reactant]). A negative $\Delta APT_{TS-Reac}$ value indicates a reduction in the positive charge on carbon and a positive $\Delta APT_{TS-Reac}$ value indicates a reduction in the negative charge on oxygen when moving from the RC to the TS. In the catalyzed TS, one C–OH bond of the nearly planar BINOL substrate is pointing towards the graphene catalyst and the other C–OH bond is pointing away from the graphene catalyst (Figure 1). Inspection of the $\Delta APT_{TS-Reac}$ values in Table 2 reveals that the $\Delta APT_{TS-Reac}$ values of the C–OH bond pointing away from the graphene catalyst are affected to a larger extent by the polarity of the solvent. In particular, on the carbon atom we obtain $\Delta APT_{TS-Reac}$ = –0.09

7

(benzene), –0.11 (diphenyl ether), –0.15 (DMF), and –0.16 (water) a.u. Similarly, on the oxygen atom we obtain $\Delta APT_{TS-Reac}$ = +0.07 (benzene), +0.08 (diphenyl ether), +0.10 (DMF and water) a.u. These results suggest that, compared to the nonpolar solvents (benzene and diphenyl ether), the polar solvents (DMF and water) allow for a greater degree of charge reorganization along the reaction coordinate which may contribute to a greater stabilization of the TS in the polar solvents. Inspection of the $\Delta APT_{TS-Reac}$ values of the reactant and TS in the uncatalyzed process (Table S1) reveals little or no difference in C–O bond polarity change between reactant and TS in the four solvents. These results are consistent with the minor solvent effects observed for the uncatalyzed reaction barrier heights.

Table 2. Solvent effects on the atomic polar tensor (APT) charges (in a.u.) on the polar C–O bond in the reactant complex and catalyzed transition structure.[a]

Atom	Benzene	Diphenyl ether	DMF	Water
C(pointing away from cat.)[b]	–0.09	–0.11	–0.15	–0.16
O(pointing away from cat.)[b]	0.07	0.08	0.10	0.10
C(pointing towards cat.)[c]	–0.10	–0.11	–0.11	–0.12
O(pointing towards cat.)[c]	0.04	0.04	0.04	0.05

[a]The tabulated values are the difference in APT charges between the TS and reactant complex ($\Delta APT_{TS-Reac}$ = [APT charge in TS] – [APT charge in reactant]). The APT charges are listed in Table S1 of the Supporting Information. [b]C–O bond pointing away from the graphene catalyst (see Figure 1). [c]C–O bond pointing towards the graphene catalyst (see Figure 1).

Nature of non-covalent interactions responsible for the catalytic activity of graphene. As illustrated in the solution-optimized structures in Figure 1, and was previously shown to be the case in the gas-phase,[8] the near-planar geometry of the inversion TS allows for both naphthyl units of the BINOL to form non-covalent π-interactions with the graphene flake, with the shortest C•••C distance between the graphene catalyst and BINOL being just 3.22 Å. (This intermolecular separation is notably shorter than those in extended polycyclic aromatic hydrocarbon dimers, such as the coronene dimer, where the separation amounts to 3.5 Å.[40,41])

8

The lower shape complementarity of the twisted equilibrium structures with the catalyst, on the other hand, results in poorer binding, with only one naphthyl unit being appropriately oriented for π-π stacking interactions.

In order to shed light on the energy components of the non-covalent interactions responsible for the catalytic effect observed here, we carried out an energy decomposition analysis using the second generation ALMO-EDA scheme by Head-Gordon and co-workers.[29] This allows us to break down the intermolecular interaction energy, ΔE_{INT}, into chemically insightful contributions from electrostatic interactions (ΔE_{ELEC}), dispersion interactions (ΔE_{DISP}), Pauli repulsion (ΔE_{PAULI}) as well as a polarization (ΔE_{POL}) and a charge transfer term (ΔE_{VCT}), as illustrated in Figure 2. We note that the EDA analysis is carried out on the CPCM(DMF)-PBE-D3BJ/6-31G(d) structures shown in Figure 2. Since these structures are very similar to those optimized in the other solvents, the solvent used in the geometry optimizations is not expected to significantly affect these results.
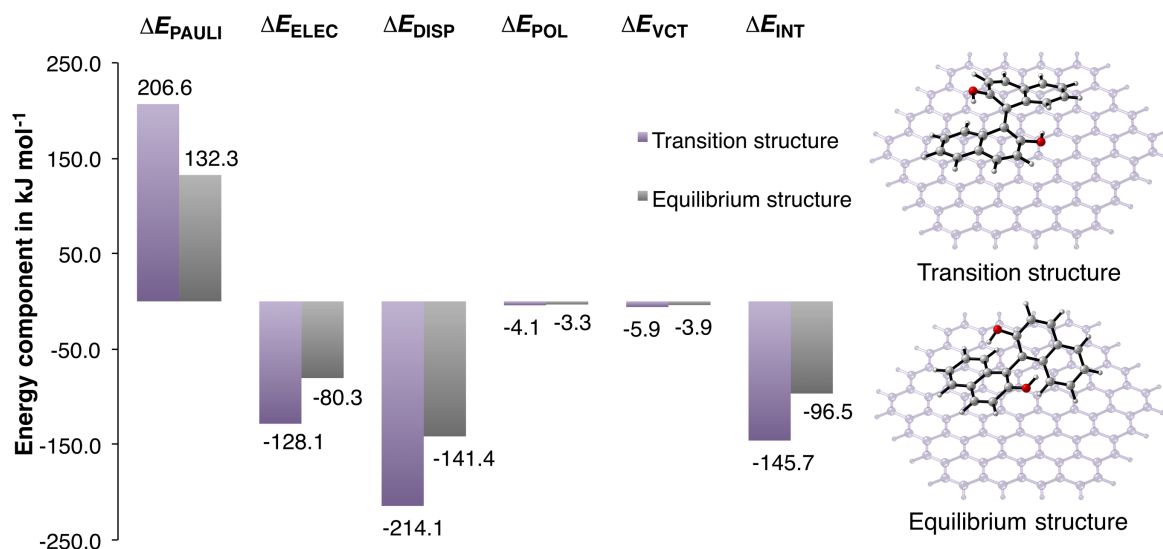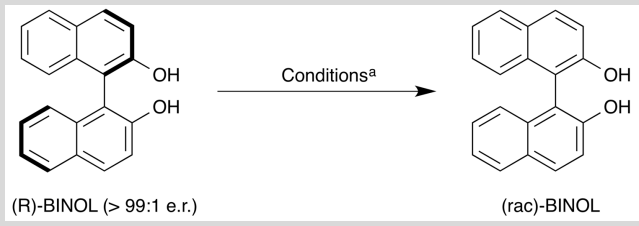
Figure 2. Breakdown of the interaction energies in the transition and equilibrium structure complexes obtained from second generation ALMO-EDA at the ωB97M-V/Def2-SVP level of theory with Hartree–Fock as the dispersion free functional.

Not unexpectedly, we find that all energy terms have a larger magnitude in the more closely interacting transition structure complex compared to the less closely bound equilibrium structure complex. In both complexes the destabilizing Pauli repulsion is outweighed by large stabilizing electrostatic and dispersion interactions, which form the main contributors to stabilization in these systems. By comparison, contributions from polarization and charge transfer are almost negligibly small. When comparing the magnitude of the stabilizing electrostatic and dispersion interactions between the two complexes, we find that both components are by over 50% larger in the transition structure complex compared to the equilibrium structure complex. Relative stabilizations of 47.8 ($\Delta\Delta E_{ELEC}$) and 72.8 kJ mol^{-1} ($\Delta\Delta E_{DISP}$) between the two complexes are observed. In agreement with previous research, these large contributions from electrostatic and dispersion interactions are typical of π-stacked aromatic systems.[42]

Experimental validation of the computational predictions. Considering the above computational predictions, we set out to provide experimental evidence for the graphene-catalyzed BINOL racemization in solution. These results are provided in Table 3. We begin the experimental exploration by identifying graphene materials that would qualify as efficient catalysts. To this end we observed the degree of racemization of enantiopure (R)-BINOL after 18h at 100 °C in the presence of 20 wt % of a range of different graphene materials. (Previous experimental studies have shown that the uncatalyzed racemization of BINOL only occurs to an appreciable extent at temperatures above 200 °C.[17])

Table 3. Experimental optimization of the catalyzed racemization of (R)-BINOL.

Entry	Catalyst (20 wt%)	Solvent	Temp. (°C)	Time	e.r.[b]
1	None	H_2O	100	18 h	>99:1
2	Graphene Nanoplatelets[c]	H_2O	"	"	95:5
3	"	DMF	"	"	>99:1
4	"	Toluene	"	"	>99:1
5	Few-layer graphene[d]	H_2O	"	"	64:36
6	Single-layer graphene[e]	H_2O	"	"	50:50
7	"	DMF	"	"	51:49
8	"	2:1 H_2O/DMF	"	"	50:50
9	"	2:1 H_2O/DMF	60	24 h	55:45

[a]Reactions were conducted with 30 mg of (R)-BINOL and 6 mg of catalyst in 5 mL of solvent, stirred in a 10 mL reaction vial for the indicated time. [b]Enantiomeric ratio determined by chiral HPLC analysis. [c]120–150 m^2/g, 6–8 nm thickness. [d]700–800 m^2/g, 1–4 nm thickness. [e]400–1000 m^2/g, 0.6–1.2 nm thickness.

Our first catalyst candidate, graphene nanoplatelets with an average thickness of 6–8 nm and a surface area of 120–150 m^2/g, proved ineffective, resulting in no racemization in toluene and DMF. Only minor racemization (5% conversion) was observed in aqueous solution (Table 3, entry 4). Expecting better catalytic ability from materials more closely resembling

the pristine graphene flake of our computational model system, we subsequently tested few- and single-layer graphene materials which led to increased catalytic activity. While few-layer graphene (700–800 m^2/g, 1–4 nm thickness) gave an enantiomeric ratio (e.r.) of 64:36 after 18h (Table 3, entry 5), single-layer graphene (400–1000 m^2/g, 0.6–1.2 nm thickness) catalyzed the complete racemization of (R)-BINOL in 18 hours (entry 6). Hereby, both DMF as well as water/DMF mixtures proved appropriate solvents, with aqueous conditions being slightly more effective. Using 2:1 water/DMF as solvent, the reaction could be carried out at 60 °C, giving BINOL with an e.r. of 55:45 after 24 hours (entry 9).

With the optimized catalyst material in hand, the Gibbs-free activation energy of the catalyzed BINOL racemization was determined experimentally. To this end we monitored the enantiopurity of a sample of (R)-BINOL over time in the presence of 20 wt% single layer graphene in H_2O/DMF solution at 60 °C, 70 °C, and 80 °C. Figure 3a shows an example of the observed changes in enantiomeric composition over time at 60 °C. As expected for a racemization, the reaction displayed clear first-order kinetics. From this data rate constants were obtained for the different temperatures (Figure 3b). The resulting Eyring plot (Figure S1 of the Supplementary Information) was used to extrapolate the Gibbs free energy barrier of the process, giving rise to a value of $\Delta G^{\ddagger}_{298} = 104.6$ kJ mol^{-1}. This experimental barrier is in good agreement with the calculated barrier in DMF (112.7 kJ mol^{-1}). We point out that, similar to the uncatalyzed barrier in diphenyl ether (*vide supra*), theory overestimates the experimental barrier height by 8.1 kJ mol^{-1} and that this difference may be partially attributed to the inclusion of solvent effects via an implicit solvation model.

12

a)

Racemization of (R)-BINOL over time at 60 °C

Legend: % (S)-BINOL; Enantiomeric excess

(Plot: Percentage vs Time (min))

b)

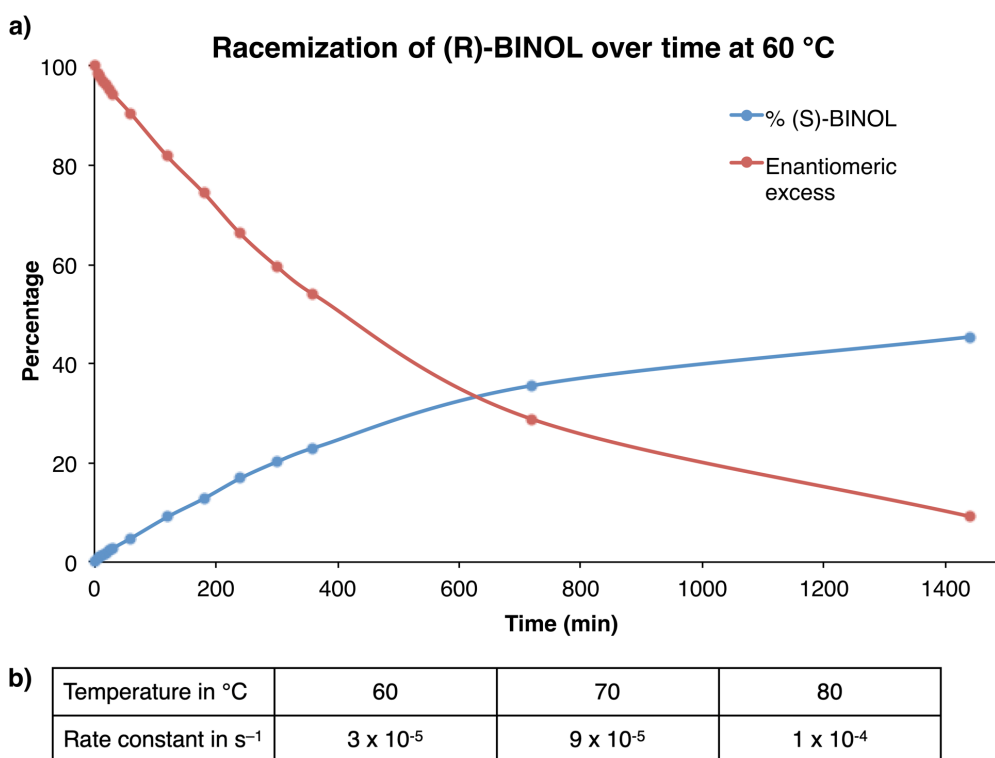| Temperature in °C	60	70	80
Rate constant in s^{-1}	3×10^{-5}	9×10^{-5}	1×10^{-4}

Figure 3. a) Plot showing the racemization of (R)-BINOL over time at 60 °C in H_2O/DMF with 20 wt% single layer graphene. b) Rate constants obtained for the racemization of (R)-BINOL in H_2O/DMF with 20 wt% single layer graphene at 60, 70, and 80 °C.

4. Conclusions

In this work we have used both computational and experimental approaches to demonstrate that single-layer graphene can efficiently catalyze the racemization of axially chiral BINOL in solution. We begin by exploring the uncatalyzed and graphene-catalyzed inversion of BINOL at the double-hybrid DFT level in a number of representative solvents of varying polarity: benzene, diphenyl ether, DMF, and water. Our calculated reaction barrier height for the uncatalyzed racemization in diphenyl ether (172.1 kJ mol^{-1}) is in good agreement with the recently determined experimental value (165.4 ± 0.3 kJ mol^{-1}). The calculated graphene-catalyzed reaction barrier heights in solution are $\Delta G^{\ddagger}_{cat}$ = 123.6 (benzene), 124.8 (diphenyl ether), 112.7 (DMF), and 115.5 (water) kJ mol^{-1}. These catalyzed barrier heights

13

correspond to catalytic efficiencies of 47.8 (benzene), 47.2 (diphenyl ether), 60.7 (DMF), and 58.0 (water) kJ mol^{-1} relative to the uncatalyzed barrier heights. These results show that pristine graphene is an efficient catalyst for the racemization of BINOL in solution. We subsequently used a DFT-based energy decomposition analysis to provide insights into the non-covalent interactions driving this catalytic activity, revealing that electrostatic and dispersion interactions are the main driving forces of this catalysis.

Based on these computational results, we proceeded to explore the graphene-catalyzed BINOL inversion experimentally and show that single-layer graphene efficiently catalyzes this process. While the uncatalyzed racemization requires high temperatures of over 200 °C, we demonstrate that single-layer graphene makes the transformation accessible at 60 °C. The experimental Gibbs free energy barrier of the process ($\Delta G^{\ddagger}_{298} = 104.6$ kJ mol^{-1}) is in reasonably good agreement with the calculated barrier in DMF (112.7 kJ mol^{-1}). We hope that the computational and experimental results presented here inspire further explorations into catalysis by pristine graphene.

Supporting Information. APT charges on the polar C–O bond in the reactant complex and catalyzed transition structure in benzene, diphenyl ether, DMF, and water (Table S1); Chiral HPLC traces (Figure S1); Kinetic data (Section S1); Eyring plot for single-layer graphene catalyzed BINOL racemization at 60, 70, and 80 °C (Figure S2); and CPCM(solvent)-PBE-D3BJ/6-31G(d) optimized geometries of all the considered structures (solvent = benzene, diphenyl ether, DMF, and water) (Table S2).

Corresponding Authors. E-Mail: joel.hooper@monash.edu (J.F.H.); amir.karton@uwa.edu.au (A.K.).

References

[1] L. Pauling, *Nature* **1948**, *161*, 707.

[2] A. J. Neel, M. J. Hilton, M. S. Sigman, F. D. Toste, *Nature* **2017**, *543*, 637.

[3] F. D. Toste, M. S. Sigman, S. J. Miller, *Acc. Chem. Res.* **2017**, *50*, 609.

[4] J. P. Wagner, P. R. Schreiner, *Angew. Chem. Int. Ed.* **2015**, *54*, 12274.

[5] H.-J. Schneider, *Angew. Chem. Int. Ed.* **2009**, *48*, 3924.

[6] V. V. Gobre, A. Tkatchenko, *Nat. Commun.* **2013**, *4*, 2341.

[7] A. Karton, *Chem. Phys. Lett.* **2014**, *614*, 156.

[8] A. A. Kroeger, A. Karton, *J. Org. Chem.* **2019**, *84*, 11343.

[9] P. A. Denis, *J. Phys. Chem. A* **2015**, *119*, 5770.

[10] D. Parmar, E. Sugiono, S. Raja, M. Rueping, *Chem. Rev.* **2014**, *114*, 9047.

[11] Y. Chen, S. Yekta, A. K. Yudin, *Chem. Rev.* **2003**, *103*, 3155.

[12] J. M. Brunel, *Chem. Rev.* **2007**, *107*, PR1.

[13] G. Ma, M. P. Sibi, *Chem. Eur. J.* **2015**, *21*, 11644.

[14] G. A. I. Moustafa, Y. Oki, S. Akai, *Angew. Chem. Int. Ed.* **2018**, *57*, 10278.

[15] J. D. Jolliffe, R. J. Armstrong, M. D. Smith, *Nat. Chem.* **2017**, *9*, 558.

[16] V. Bhat, S. Wang, B. M. Stoltz, S. C. Virgil, *J. Am. Chem. Soc.* **2013**, *135*, 16829.

[17] D. C. Patel, R. M. Woods, Z. S. Breitbach, A. Berthod, D. W. Armstrong, *Tetrahedron: Asymmetry* **2017**, *28*, 1557.

[18] J. P. Perdew, K. Burke, M. Ernzerhof, *Phys. Rev. Lett.* **1996**, *77*, 3865; *ibid*, **1997**, *78,* 1396.

[19] K. Raghavachari, J. S. Binkley, R. Seeger, J. A. Pople, *J. Chem. Phys.* **1980**, *72*, 650.

[20] S. Grimme, *WIREs Comput. Mol. Sci.* **2011**, *1*, 211.

[21] A. D. Becke, E. R. Johnson, *J. Chem. Phys.* **2005**, *123*, 154101.

[22] M. Cossi, N. Rega, G. Scalmani, V. Barone, *J. Comput. Chem.* **2003**, *24*, 669.

[23] C. Gonzalez, H. B. Schlegel, *J. Chem. Phys.*1989, *90*, 2154.

[24] M. J. Frisch, G. W. Trucks, H. B. Schlegel, G. E. Scuseria, M. A. Robb, J. R. Cheeseman, G. Scalmani, V. Barone, G. A. Petersson, H. Nakatsuji, X. Li, M. Caricato, A. V. Marenich, J. Bloino, B. G. Janesko, R. Gomperts, B. Mennucci, H. P. Hratchian, J. V. Ortiz, A. F. Izmaylov, J. L. Sonnenberg, D. Williams-Young, F. Ding, F. Lipparini, F. Egidi, J. Goings, B. Peng, A. Petrone, T. Henderson, D. Ranasinghe, V. G. Zakrzewski, J. Gao, N. Rega, G. Zheng, W. Liang, M. Hada, M. Ehara, K. Toyota, R. Fukuda, J. Hasegawa, M. Ishida, T. Nakajima, Y. Honda, O. Kitao, H. Nakai, T. Vreven, K. Throssell, J. A. Montgomery, Jr.., J. E. Peralta, F. Ogliaro, M. J. Bearpark, J. J. Heyd, E. N. Brothers, K. N. Kudin, V. N. Staroverov, T. A. Keith, R. Kobayashi, J. Normand, K. Raghavachari, A. P. Rendell, J. C. Burant, S. S. Iyengar, J. Tomasi, M. Cossi, J. M. Millam, M. Klene, C. Adamo, R. Cammi, J. W. Ochterski, R. L. Martin, K. Morokuma, O. Farkas, J. B. Foresman, D. J. Fox, Gaussian 16, Revision A.03, Gaussian, Inc., Wallingford, CT, 2016.

[25] G. Santra, N. Sylvetsky, J. M. L. Martin, *J. Phys. Chem. A* **2019**, *123*, 5129.

[26] J. M. L. Martin, G. Santra, *Isr. J. Chem.*, **2020**, *Early View*, DOI: 10.1002/ijch.201900114.

[27] F. Weigend, R. Ahlrichs, *Phys. Chem. Chem. Phys.* **2005**, *7*, 3297.

[28] F. Neese, *WIREs Comput. Mol. Sci.* **2011**, *2*, 73.

[29] P. R. Horn, Y. Mao, M. Head-Gordon, *Phys. Chem. Chem. Phys.* **2016**, *18*, 23067.

[30] N. Mardirossian, M. Head-Gordon , *J. Chem. Phys.* **2016**, *144*, 214110.

[31] Y. Shao, Z. Gan, E. Epifanovsky, A. T. B. Gilbert, M. Wormit, J. Kussmann, A. W. Lange, A. Behn, J. Deng, X. Feng, D. Ghosh, M. Goldey P. R. Horn, L. D. Jacobson, I. Kaliman, R. Z. Khaliullin, T. Kús, A. Landau, J. Liu, E. I. Proynov, Y. M. Rhee, R. M. Richard, M. A. Rohrdanz, R. P. Steele, E. J. Sundstrom, H. L. Woodcock III, P. M. Zimmerman, D. Zuev, B. Albrecht, E. Alguire, B. Austin, G. J. O. Beran, Y. A. Bernard, E. Berquist, K. Brandhorst, K. B. Bravaya, S. T. Brown, D. Casanova, C.-M. Chang, Y. Chen, S. H. Chien, K. D. Closser, D. L. Crittenden, M. Diedenhofen, R. A. DiStasio Jr., H. Dop, A. D. Dutoi, R. G. Edgar, S. Fatehi, L. Fusti-Molnar, A. Ghysels, A. Golubeva-Zadorozhnaya, J. Gomes, M. W. D. Hanson-Heine, P. H. P. Harbach, A. W. Hauser, E. G. Hohenstein, Z. C. Holden, T.-C. Jagau, H. Ji, B. Kaduk, K. Khistyaev, J. Kim, J. Kim, R. A. King, P. Klunzinger, D. Kosenkov, T. Kowalczyk, C. M. Krauter, K. U. Lao, A. Laurent, K. V. Lawler, S. V. Levchenko, C. Y. Lin, F. Liu, E. Livshits, R. C. Lochan, A. Luenser, P. Manohar, S. F. Manzer, S.-P. Mao, N. Mardirossian, A. V. Marenich, S. A. Maurer, N. J. Mayhall, C. M. Oana, R. Olivares-Amaya, D. P. O'Neill, J. A. Parkhill, T. M. Perrine, R. Peverati, P. A. Pieniazek, A. Prociuk, D. R. Rehn, E. Rosta, N. J. Russ, N. Sergueev, S. M. Sharada, S. Sharmaa, D. W. Small, A. Sodt, T. Stein, D. Stück, Y.-C. Su, A. J. W. Thom, T. Tsuchimochi, L. Vogt, O. Vydrov, T. Wang, M. A. Watson, J. Wenzel, A. White, C. F. Williams, V. Vanovschi, S. Yeganeh, S. R. Yost, Z.-Q. You, I. Y. Zhang, X. Zhang, Y. Zhou, B. R. Brooks, G. K. L. Chan, D. M. Chipman, C. J. Cramer, W. A. Goddard III, M. S. Gordon, W. J. Hehre, A. Klamt, H. F. Schaefer III, M. W. Schmidt, C. D. Sherrill, D. G. Truhlar, A. Warshel, X. Xua, A. Aspuru-Guzik, R. Baer, A. T. Bell, N. A. Besley, J.-D. Chai, A. Dreuw, B. D. Dunietz, T. R. Furlani, S. R. Gwaltney, C.-P. Hsu, Y. Jung, J. Kong, D. S. Lambrecht, W. Liang, C. Ochsenfeld, V. A. Rassolov, L. V. Slipchenko, J. E. Subotnik, T. Van Voorhis, J. M. Herbert, A. I. Krylov, P. M. W. Gill, and M. Head-Gordon. Advances in molecular quantum chemistry contained in the Q-Chem 4 program package.

[32] Y. H. Shao, Z. T. Gan, E. Epifanovsky, A. T. B. Gilbert, M. Wormit, J. Kussmann, A. W. Lange, A. Behn, J. Deng, X. T. Feng, D. Ghosh, M. Goldey, P. R. Horn, L. D. Jacobson, I. Kaliman, R. Z. Khaliullin, T. Kus, A. Landau, J. Liu, E. I. Proynov, Y. M. Rhee, R. M. Richard, M. A. Rohrdanz, R. P. Steele, E. J. Sundstrom, H. L. Woodcock, P. M. Zimmerman, D. Zuev, B. Albrecht, E. Alguire, B. Austin, G. J. O. Beran, Y. A. Bernard, E. Berquist, K. Brandhorst, K. B. Bravaya, S. T. Brown, D. Casanova, C. M. Chang, Y. Q. Chen, S. H. Chien, K. D. Closser, D. L. Crittenden, M. Diedenhofen, R. A. DiStasio, H. Do, A. D. Dutoi, R. G. Edgar, S. Fatehi, L. Fusti-Molnar, A. Ghysels, A. Golubeva-Zadorozhnaya, J. Gomes, M. W. D. Hanson-Heine, P. H. P. Harbach, A. W. Hauser, E. G. Hohenstein, Z. C. Holden, T. C. Jagau, H. J. Ji, B. Kaduk, K. Khistyaev, J. Kim, J. Kim, R. A. King, P. Klunzinger, D. Kosenkov, T. Kowalczyk, C. M. Krauter, K. U. Lao, A. D. Laurent, K. V. Lawler, S. V. Levchenko, C. Y. Lin, F. Liu, E. Livshits, R. C. Lochan, A. Luenser, P. Manohar, S. F. Manzer, S. P. Mao, N. Mardirossian, A. V. Marenich, S. A. Maurer, N. J. Mayhall, E. Neuscamman, C. M. Oana, R. Olivares-Amaya, D. P, J. A. Neill, T. M. Parkhill, R. Perrine, A. Peverati, D. R. Prociuk, E. Rehn, N. J. Rosta, S. M. Russ, S. Sharada, D. W. Sharma, A. Small, T. Sodt, D. Stein, Y. C. S. Stuck, A. J. W. Thom, T. Tsuchimochi, V. Vanovschi, L. Vogt, O. Vydrov, T. Wang, M. A. Watson, J. Wenzel, A. White, C. F. Williams, J. Yang, S. Yeganeh, S. R. Yost, Z. Q. You, I. Y. Zhang, X. Zhang, Y. Zhao, B. R. Brooks, G. K. L. Chan, D. M. Chipman, C. J. Cramer, W. A. Goddard, M. S. Gordon, W. J. Hehre, A. Klamt, H. F. Schaefer, M. W. Schmidt, C. D. Sherrill, D. G. Truhlar, A. Warshel, X. Xu, A. Aspuru-Guzik, R. Baer, A. T. Bell, N. A. Besley, J. D. Chai, A. Dreuw, B. D. Dunietz, T. R. Furlani, S. R. Gwaltney, C. P. Hsu, Y. S. Jung, J. Kong, D. S. Lambrecht, W. Z. Liang, C. Ochsenfeld, V. A. Rassolov, L. V. Slipchenko, J. E. Subotnik, T. Van Voorhis, J. M. Herbert, A. I. Krylov, P. M. W. Gill, M. Head-Gordon, Mol. Phys. **2015**, *113*, 184.

[33] C. Y. Legault, CYLview, 1.0b; Université de Sherbrooke, 2009; http://www.cylview.org.

[34] L. Meca, D. Reha, Z. Havlas, *J. Org. Chem.* **2003**, *68*, 5677.

[35] L.-G. Da, J. He, L.-F. Hu, *J. Phys. Org. Chem.* **2019**, *32*, e3900.

[36] N. V. Tkachenko, S. Scheiner, *ACS Omega* **2019**, *4*, 6044.

[37] J. Cioslowski, *J. Am. Chem. Soc.* **1989**, *111*, 8333.

[38] F. De Proft, J. M. L. Martin, P. Geerlings, *Chem. Phys. Lett.* **1996**, 250, 393.

[39] M. Cho, N. Sylvetsky, S. Eshafi, G. Santra, I. Efremenko, J. M. L. Martin, *ChemPhysChem* **2020**, *21*, 688.

[40] R. Podeszwa, *J. Chem. Phys.* **2010,** *132*, 044704.

[41] T. Janowski, A. R. Ford, P. Pulay, *Mol. Phys.* **2010**, *108*, 249.

[42] S. Grimme, *Angew. Chem. Int. Ed.* **2008**, *47*, 3430.